Revision 2

Ultra-deep subduction of Yematan eclogite in the North Qaidam UHP belt, NW China: evidence from phengite exsolution in omphacite

Lei Han, Lifei Zhang* and Guibin Zhang

MOE Key Laboratory of Orogenic Belts and Crustal Evolution, School of Earth and Space Sciences, Peking University, Beijing, China

(* corresponding author: lfzhang@pku.edu.cn)

ABSTRACT

Phengite exsolution in omphacite from the Yematan eclogite, North Qaidam UHP belt, NW China, is described. Mineralogical investigations show that the precursor omphacite in the Yematan eclogite contains up to 1.16 wt% K_2O and ~10000 ppm H_2O. Experimental studies document this omphacite to be formed at pressures higher than 6 GPa (at 900°C). The pressure-temperature conditions of 3.68 GPa and 892 °C for phengite exsolution in omphacite associated with garnet during the exhumation were obtained by using Grt–Omp–Ph geothermobarometer. We conclude that omphacitic-clinopyroxene in subducted eclogites may act as a robust medium to transport H_2O and potassium deep into the interior of the Earth. This study suggests that the Yematan eclogite in North Qaidam UHP metamorphic belt, NW China, may have been subducted and exhumed from depths of more than 200 km.

Keywords: Phengite exsolution, eclogite, ultra-deep subduction, North Qaidam, China

INTRODUCTION

Since Switzer and Melson (1969) found 0.3 wt% K_2O in pyroxene from a diamond-bearing eclogite from the Roberts Victor Mine, potassium-rich clinopyroxenes and exsolved potassium-mineral lamellae in clinopyroxenes have been extensively reported from ultra-high pressure (UHP) rocks. For example, some eclogitic omphacites (Reid et al. 1976; Harlow and Veblen 1991; Xiao et al. 2000), as well as clinopyroxenes from carbonate (Sobolev and Shatsky 1990; Ogasawara et al. 2002) and ultra-basic rocks (Bindi et al. 2003) were reported to contain unexpectedly high potassium abundances. Potassium-bearing minerals have also exsolved in clinopyroxenes from calcsilicate rocks (Katayama et al. 2002; Zhu and Ogasawara 2002; Bozhilov et al. 2009; Schertl and Sobolev 2013) and eclogites (Schmädicke and Müller 2000). Moreover, according to studies of diamond-bearing eclogite xenoliths (Reid et al. 1976; Harlow and Veblen 1991; Okamoto et al. 2000), as well as from experiments (Harlow 1997; Luth 1997; Okamoto and Maruyama 1998; Wang and Takahashi 1999), it is known that potassium-rich (>1 wt% K_2O) clinopyroxene is stable at pressures above 6 GPa. For example, there is ~1 wt% K_2O in subsolidus clinopyroxene at 6 GPa (Wang and Takahashi 1999).

The North Qaidam UHP metamorphic belt in northwestern China consists of three coesite-bearing eclogite terranes and one diamond-bearing garnet peridotite terrane. The coesite-bearing terrances, from west to east are the Yuka, Xitieshan, and Dulan; the diamond-bearing rocks are represented by the Lüliangshan peridotite terrane (Fig. 1a). To date, the Lüliangshan peridotite terrane has been confirmed to have been subducted to depths greater than 200 km (Song et al. 2004, 2005); for the other three coesite-bearing eclogite terranes, depths of ~100 km have been suggested (Zhang et al. 2009a, 2009b; Zhang et al. 2009; Liu et al. 2012). Potassium-bearing mineral exsolution in eclogite is rarely reported. Phlogopite exsolution lamellae in eclogitic garnet from the No.50 kimberlite pipe of Fuxian County, Liaoning Province, China (Zhou 1997) and potassium-white mica lamellae in omphacite from the Erzgebirge crystalline complex (Schmädicke and Müller, 2000) have been qualitatively identified by transmission

electron microscope (TEM) and energy dispersive X-ray spectrometry (EDX). Here we report phengite exsolution in omphacite from two eclogite samples and discuss its implication for ultra-deep subduction of the Yematan UHP terrane, NW China.

GEOLOGICAL SETTING AND SAMPLE DESCRIPTION

The Yematan UHP terrane is located in the eastern part of the North Qaidam ultrahigh pressure (UHP) metamorphic belt (Fig. 1). The North Qaidam UHP belt (Song et al. 2003) is located in northwestern China and contains four metamorphic terranes (Fig. 1a). From east to west: they are the Dulan terrane; the Xitieshan terrane; the Lüliangshan terrane; and the Yuka terrane.

The Yematan eclogite and peridotite occur as blocks, boudins or layers in host para- and ortho-gneiss. The discovery of coesite inclusion in zircon from the Yematan host paragneiss indicates that Yematan eclogitic rocks may have been subjected to UHP metamorphism (Yang et al. 2001). Two eclogite samples (11ym26 and 12ym05) with phengite exsolution in omphacite were collected in the Yematan area. They occur with four types of eclogites (bimineralic eclogite, phengite-epidote eclogite, phengite eclogite and epidote eclogite), serpentinized peridotite (some peridotite contain relic HP garnet; Mattinson et al. 2007), garnet-bearing pyroxenite (Song et al. 2003), and the host para- and ortho-gneiss. The two eclogite samples (Fig. 1 b) with phengite exsolution in omphacite, 11ym26 and 12ym05, consist of garnet (35-40%) + omphacite (30-40%) + quartz (5%) + rutile (5%) + phengite (2%), with up to 10% amphibole + plagioclase or diopside + albite symplectite after garnet or omphacite respectively (Fig. 2). All phengite occur as inclusions in the host omphacite and no phengite was observed in the matrix or as inclusions in garnet. Both eclogites display medium to coarse grain textures. Garnets have coronas of Amp + Pl; edges of some matrix omphacites are replaced by Di + Ab symplectites. Some omphacite grains contain abundant phengite lamellae that are oriented parallel to the direction of {100} cleavage in omphacite (Fig. 2 c-f). The phengite lamellae typically have widths ranging from less than 1 to 5 μm (Fig. 2 c-f). Based on the petrographical observation above, three metamorphic

stages can be distinguished: the peak stage for the formation of H_2O- and potassium-bearing omphacite (stage I), the exsolution of phengite in omphacite associated with garnet during the early exhumation (stage II) and the retrograde amphibolite facies for the symplectic Amp + Pl after the stage II.

MINERAL COMPOSITIONS

Electron probe microanalyses (EPMA) of minerals (Table 1 and 2), including exsolution lamellae in the two samples (Table 3), were obtained using a JEOL JXA-8230 at the Key Laboratory of Metallogeny and Mineral Assessment of MLR, Institute of Mineral Resources, Beijing, China. Mineral compositions were quantitatively analyzed at acceleration voltage of 15 kV with a beam current of 20 nA. A ZAF correction was applied during data reduction. Standards used for instrument calibration include jadeite (Na, Al and Si), forsterite (Mg), K-feldspar (K), wollastonite (Ca), hematite (Fe), rutile (Ti), Cr_2O_3 (Cr), and MnO (Mn). Analytical precision of mineral compositions is better than ± 2% for SiO_2, Al_2O_3, FeO, MgO, CaO, K_2O and Na_2O, for TiO_2, Cr_2O_3, and MnO < ± 10%.

Garnet and omphacite

In eclogite sample 11ym26, garnet compositions are almandine 42–46 mole%, pyrope 24–27 mole% and grossular 25–32 mole%, and omphacite with exsolution lamellae has 45–50 mole% jadeite (Table 1 and 2). Garnet in the sample 12ym05 is characterized by higher MgO and lower FeO contents and with irregular compositional variation (almandine 36–41 mole%, pyrope 30–36 mole%, grossular 25–33 mole%). The jadeite content of matrix omphacite in the sample 12ym05 with exsolution lamellae ranges from 34 to 40 mole% (Table 1). A few garnets, typically those in contact with quartz, may retain their primary rim compositions characterized by a relatively high pyrope content.

Exsolution lamellae

Based on the EPMA of exsolution lamellae which are big enough to provide data and not contaminated by the host omphacite, they are phengite with Si contents varying from 3.45 to 3.67 a.p.f.u. (Table 3). Furthermore, the Si contents of omphacite domains, which contain phengite exsolutions, are a bit lower than that of the pre-exsolution omphacite (typically <1.95 a.p.f.u. versus ~1.98 a.p.f.u. respectively) (Tables 2 and 3).

EBSD ANALYSIS

Electron back-scatter diffraction (EBSD) measurements were carried out in the Environmental SEM Laboratory, Peking University using a Nodlys S^+-type EBSD system mounted on a FEI Quanta 650 FEG-type SEM. Experimental conditions were a 20 kV accelerating voltage, 15.0 mm working distance and 70° tilting of the specimen (plane polished thin section). The EBSD technique uses electrons diffracted from the unit-cell layers closest to the surface, which are detected on a phosphor screen. The light bands on the collected images are Kikuchi bands (Fig. 4a, b) and reflect the three-dimensional orientation of lattice planes in the crystalline target. The quality of the image depends on several factors, of which perhaps the quality of the polishing of the sample surface is the most critical; the quality of the patterns may also be impacted by mineral composition and lattice structure (Ullemeyer et al. 2000). Diffraction image of phengite (Fig. 4b) has lower quality than that of omphacite (Fig. 4b). The crystallographic orientation of phengite exsolution lamellae and the omphacite host were measured and plotted in a stereographic pole figure (LPO, lattice preferred orientations; Fig. 4c, d). The orientation of phengite's a-axis is parallel to the orientation of omphacite's c-axis, and a relationship described as $[001]_{omp} \parallel [100]_{ph}$ is concluded.

PRESSURE-TEMPERATURE ESTIMATES

The peak stage of H_2O- and potassium-bearing omphacite before the exsolution (stage I)

To estimate the initial composition of the omphacite prior to phengite exsolution, exsolved

phases identified by microscopic observation and EBSD analyses (Fig. 2; Fig. 4) were compositionally reintegrated by measuring their areal proportions on digital images. Based on the calculated areas of phengite lamellae and host omphacite (Fig. 2d-f), the composition of the pre-exsolution omphacite may be estimated by mixing ~3-15% phengite and ~85-97% host omphacite. Based on EPMA of phengite lamellae and host omphacite (Tables 1 and 2), it is estimated that the precursor phase may have contained between 0.4 and 1.16 wt% K_2O with an average of about 1.09 wt%, and up to 1.05 wt% H_2O with an average of about 0.3 wt%, which corresponds to more than 10000 ppm H_2O with an average of about 3000 ppm. However, water abundance was estimated indirectly by presuming that the volatile in phengite is only H_2O and the effect of H_2O : CO_2 ratio on the stability of phengite has also not been considered. Therefore, the water abundance may be overestimated. The crystallographic site of potassium in phengite is only half filled (K=0.41 to 0.65 atoms pfu; Table 3). Based on the high-pressure experimental studies (Harlow 1997; Luth 1997; Okamoto and Maruyama 1998; Wang and Takahashi 1999), the minimum pressure of potassium-bearing omphacite in Yematan eclogite is about 6 GPa (Fig. 5a) and the potassium could be an important constituent of clinopyroxenes only at pressure >4 GPa (e.g., Harlow and Davies 2004). For example, in melting experiments of diopside-phlogopite system, clinopyroxene with 0.9 wt% K_2O is stable at 9 GPa and 1450°C (Luth 1997). Subsolidus experiments of a K-rich basaltic composition suggested that pyroxenes with ~1.0 wt% K_2O should be stable at ~6 GPa (Wang and Takahashi 1999; see Fig. 5a) and high-pressure experiments in the dioposide + kosmochlor + K_2CO_3 system synthesized a clinopyroxene with 1.0 wt% K_2O at 7 GPa and 1500°C (Harlow 1997).

Hydroxyl-bearing clinopyroxenes have been found in UHP rock worldwide and synthesized in high-pressure and high-temperature experiments. For example, clinopyroxenes in eclogites from the Kokchetav UHP terrane studied using infrared Spectroscopy were found to contain up to 3020 ppm OH (Katayama and Nakashima 2003). The cores of the clinopyroxenes in these eclogites contain up to 1 wt% K_2O and yield PT estimates of >6 GPa and > 1000°C based on

the K_2O-in-clinopyroxene geobarometer from experiments and garnet-clinopyroxene geothermometer (Okamoto et al. 2000; Wang and Takahashi 1999). Moreover, water contents in synthetic pyroxenes determined by Fourier transform infrared spectroscopy vary from ~101 ppm at 2.5 GPa and 1175°C to ~2754 ppm at 9 GPa and 1175°C in the MFSH (MgO-FeO-SiO_2-H_2O) experimental system with H_2O initial abundance of 2 wt% (Férot and Bolfan-Casanova 2012). Therefore, the precursor phase of omphacite with an average of about 3000 ppm from Yematan eclogite may have been stable at pressures > 6 GPa, which is consistent with the stable pressure of potassium-bearing omphacite above.

The retrograde metamorphic stage of exsolution of phengite in omphacite associated with garnet during the exhumation (stage II)

The Grt–Omp–Ph geothermobarometer by Ravna and Terry (2004) was used to calculate the metamorphic conditions of the eclogite using the highest $Mg/(Mg + Fe^{2+})$-value at or close to garnet rims (Carswell et al. 1997). Omphacite displayed symplectite textures may have modified compositions and thus clinopyroxene with the highest Jd content (Holland 1980) and phengite with the highest Si content were selected for the thermobarometric calculations. Mineral compositions chosen for P-T calculation represent grains that are in contact each other. The intersection of the Grt–Cpx thermometer and Grt–Ph–Cpx barometer curves yield pressures and temperatures of 3.68 GPa, 892 °C and 3.33 GPa, 857 °C for eclogite samples 12ym05 and 11ym26, respectively (Fig. 3). These PT conditions may reflect the formation of exsolved phengite in omphacite during the exhumation of the Yematan eclogite.

DISCUSSION

Ultra-deep origin of (Potassium + hydroxyl)-rich clinopyroxenes and its significance

When rocks metamorphosed during ultra-deep subduction are exhumed, exsolution phenomenon may reflect preceding ultrahigh-pressure (UHP) metamorphism of its host rock (e.g., Liou et al. 1998). For example, coesite exsolution in titanite from impure calcite marble in the

Kokchetav massif and omphacite from eclogite in western Tianshan shows that the peak UHP metamorphic pressures may have been 5.0 to 6.0 GPa (Ogasawara et al. 2002; Zhang et al. 2005). Moreover, potassium-clinopyroxenes containing up to 1.0 wt% K_2O from diamond-bearing eclogite in the Kokchetav massif (Okamoto et al. 2000) suggest that these rocks were likely stable at pressures higher than 6.0 GPa. Clinopyroxene with substantial K_2O (~0.5 to 1.9 wt%) may be stabilized at ~5.0 to 12.5 GPa according to the correlation between pressure and potassium content in high-pressure synthetic subsolidus clinopyroxene (Tsuruta and Takahashi 1998; Wang and Takahashi 1999). As a consequence, potassium-rich clinopyroxene might exsolve during uplift and decompression. For example, Katayama et al. (2002) described phengite exsolution in low-K matrix diopsides of a diamond-bearing marble. Such phengite exsolutions are thought to have formed at the expense of the potassium-jadeite and Ca-Eskola components during decompression (e.g., Schertl and Sobolev 2013). Exsolution lamellae of hydrous phases (e.g., micas) in clinopyroxenes (Schmädicke and Müller 2000; Zhu and Ogasawara 2002; Katayama et al. 2002; Bozhilov et al. 2009) were suggested to represent a genuine exsolution texture rather than interaction with a fluid phase during exhumation. Until now, the maximum reported amount of H_2O in natural clinopyroxene was 3020 ppm in eclogites from Kokchetav (Katayama and Nakashima, 2003); other studies have reported lower abundances (Smyth et al. 1991, 1800 ppm; Katayama et al. 2002, 1000 ppm; Ogasawara et al. 2002, 1000 ppm). Nominally anhydrous minerals such as clinopyroxene may contain significant amounts of H_2O and make an important contribution to water recycling deep inside of the Earth. Water recycling in subduction zones may change the rheologic properties of the mantle and may induce many other geological activities such as magmatism and earthquakes (e.g., Peacock 1990; Ernst 2001; Katayama et al. 2006). For example, persistence of hydroxyl-bearing layer silicates may explain the metastable preservation of low-density assemblages in continental crust subjected to UHP conditions (Ernst 2001), and H_2O released by metamorphic reactions in the subducting oceanic crust may alter the bulk composition in the overlying mantle

wedge and trigger partial melting reactions at greater depths (Peacock 1990). Moreover, Katayama et al. (2006) suggested that water transported by deep subducted oceanic crust may provide a repository for volatiles in the mantle and consequently play an important role in the mantle dynamics of the Earth's interior.

Potassium-bearing clinopyroxene may also an important K carrier in the deep earth and ^{40}K could be an important heat source during the evolution of the Earth (e.g., Wang and Takahashi 1999). Experiments conducted at 1-3 GPa and temperatures above the liquidus in the Fe-metal + FeS + K-silicate glass ± natural peridotite (KLB-1) system, suggested that potassium enters iron sulphide melts in a strongly temperature-dependent fashion and ^{40}K may serve as a substantial heat source in the cores of the Earth, and it seems possible that radioactive heat due to ^{40}K can affect the thermal evolution and global processes in the Earth (Murthy et al. 2003). Even subduction of K may not impact thermal budget in the core directly, it will make a contribution to K recycling deep inside of the Earth.

Ultra-deep subduction of the Yematan eclogite terrane

The minimum PT conditions of an early exhumation stage are given by Yematan eclogite sample 11ym26 (stage II; 892°C at 3.68 GPa estimated by Grt–Omp–Ph geothermobarometry applied to exsolved phengite + host omphacite + garnet in the two investigated eclogite samples) (Figs. 3 and 5). Thick-black lines in Fig. 5 are the limits of free water in mid-ocean ridge basalt (MORB) composition. Oceanic crust releases most of its H_2O by the amphibolite-eclogite transformation at ~75 km depth and reaches solidus temperatures, causing the partial melting of amphibole-bearing metamorphosed oceanic crust, at temperatures above 650 °C. The released H_2O moves into the melt and the remaining subducting oceanic crust transforms to dry eclogite (Okamoto and Maruyama 1999), but the temperature of a steady-state mantle at 6.0 GPa is higher than 1200°C (Akaogi et al. 1989); the subducted crust, however, should have had a lower temperature than the abutting mantle. Therefore, according to the discussion above, pre-exsolution omphacite from the Yematan eclogite with K_2O contents up to 1.16 wt% and at

least 0.3 wt% H_2O should have been possible in an ultrahigh-pressure environment (stage I, > 6.0 GPa, ~ 900 – 1200 °C; Fig. 5). It implies that the Yematan eclogite terrane once subducted into an ultra-deep depths of more than 200 km.

Potassium and hydroxyl in the precursor omphacite from Yematan eclogite might originate from a melt/fluid during subduction, which could have been derived from hydrous partial melting of the surrounding coesite-bearing paragneiss with its potassium and H_2O being incorporated into omphacite at high pressure. There should be some relics if the eclogite was infiltrated by the K- and H_2O-bearing melt/fluid from surrounding gneiss. However, we didn't observe any intergranular K-bearing minerals, for example, phengite, K-feldspar and K-cymrite in the two samples (11ym26 and 12ym05). Alternatively, maybe the protolith is K-rich alkali basalt, and the K-bearing melt/fluid might have been derived form the eclogite itself by dehydration of phengite. The potassium and H_2O would not be stored in phengite when the eclogite subducted to the depth with temperature >1000°C, where phengite will disappear (Schmidt 1996) but K-bearing omphacite could survive (Wang and Takahashi 1999). Phengite in the eclogite might have been exhausted through hydrous partial melting during subduction finally and this might be the reason that there is no relic found in the matrix.

CONCLUSIONS

Phengite exsolution in omphacite has been found in the Yematan eclogite, North Qaidam UHP belt, NW China. A mineralogical study shows that the precursor omphacite in the Yematan eclogite contains up to 1.16 wt% K_2O and ~10000 ppm H_2O, and may have been stable at pressures higher than 6.0 GPa and temperatures of 900°C. The phengite exsolution in the host omphacite-clinopyroxene happen at the PT conditions of 3.68 GPa and 892 °C during the exhumation of host eclogite based on the Grt–Omp–Ph geothermobarometer. We conclude that omphacitic-clinopyroxene in subducted eclogites may act as a robust medium to transport H_2O and potassium deep into the interior of the Earth.

ACKNOWLEDGMENTS

This study was financially supported by Major State Basic Research Development Program (Grant 2015CB856105) and National Science Foundation of China (Grants 41121062, 41272069, 41272068 and 410090371). We also want to give our thanks to Drs. Hans-Peter Schertl, Sébastien Potel and Callum Hetherington for their careful reviews and constructive comments on the first version.

REFERENCES CITED

Akaogi, M., Ito, E., and Navrotsky, A. (1989) Olivine-modified spinel-spinel transitions in the system Mg2SiO4-Fe2SiO4: calorimetric measurements, thermochemical calculation, and geophysical application. Journal of Geophysical Research, 94, 15671–15685.

Auzanneau, E., Vielzeuf, D., and Schmidt, M.W. (2006) Experimental evidence of decompression melting during exhumation of subducted continental crust. Contributions to Mineralogy and Petrology, 152, 125–148.

Bindi, L., Safonov, O.G., Yapaskurt, V.O., Perchuk, L.L., and Menchetti, S. (2003) Ultrapotassic clinopyroxene from the Kumdy-Kol microdiamond mine, Kokchetav Complex, Kazakhstan: Occurrence, composition and crystal-chemical characterization. American Mineralogist, 88, 464–468.

Bozhilov, K.N., Xu, Z., Dobrzhinetskaya, L.F., Jin, Z.M., and Green, H.W. (2009) Cation-deficient phlogopitic mica exsolution in diopside from garnet peridotite in SuLu, China. Lithos, 109, 304–313.

Carswell, D.A., O'Brien, P.J., Wilson, R.N., and Zhai, M.G. (1997) Thermobarometry of phengite-bearing eclogites in the Dabie Mountains of Central China. Journal of Metamorphic Geology, 15, 239–252.

Ernst, W.G. (2001) Subduction, ultrahigh-pressure metamorphism, and regurgitation of buoyant crustal slices-implications for arcs and continental growth. Physics of the Earth and Planetary Interiors, 127, 253-275.

Férot, A., and Bolfan-Casanova, N. (2012) Water storage capacity in olivine and pyroxene to 14 GPa: Implications for the water content of the Earth's upper mantle and nature of seismic discontinuities. Earth and Planetary Science Letters, 349-350, 218-230.

Harlow, G. E. (1997) K in clinopyroxene at high pressure and temperature: An experimental study. American Mineralogist, 82, 259–269.

Harlow, G. E., and Davies, R. (2004) Status report on stability of K-rich phases at mantle conditions. Lithos, 77, 647– 653.

Harlow, G. E., and Veblen B. R. (1991) Potassium in clinopyroxene: Inclusions from diamonds. Science, 251,652-655.

Holland, T.J.B. (1980) Reaction albite = jadeite + quartz determined experimentally in the range 600–1200℃. American Mineralogist, 65, 129-134.

Katayama, I., Ohta, M., and Ogasawara, Y. (2002) Mineral inclusions in zircons from diamond-bearing marble in the Kokchetav Massif, northern Kazakhstan. European Journal of Mineralogy, 14, 1103–1108.

Katayama, I., and Nakashima, S. (2003) Hydroxyl in clinopyroxene from the deep subducted crust: Evidence for H2O transport into the mantle. American Mineralogist, 88, 229–234.

Katayama, I., Nakashima, S., and Yurimoto, H. (2006) Water content in natural eclogite and its implication for water transport into the deep upper mantle. Lithos, 86, 245–259.

Liou, J.G., Zhang, R.Y., Ernst, W.G., Rumble, III D., and Maruyama, S. (1998) High-pressure minerals from deeply subducted metamorphic rocks. In R.J. Hemley, Ed., Ultrahigh-pressure mineralogy, p. 33-96. Mineralogical Society of America, Washington.

Liu, X.C., Wu, Y.B., Gao, S., Liu, Q., Wang, H., Qin, Z.W., Li, Q.L., Li, X.H., and Gong, H.J. (2012) First record and timing of UHP metamorphism from zircon in the Xitieshan terrane: implications for the evolution of the entire North Qaidam metamorphic belt. American Mineralogist, 97, 1083–1093.

Luth, R. W. (1997) Experimental study of the system phlogopite-diopside from 3.5—17 GPa.

American Mineralogist, 82, 1198–1209.

Mattinson, C.G., Menold, C.A., Zang, J.X., and Bird, D.K. (2007) High- and ultrahigh-pressure metamorphism in the North Qaidam and South Altyn Terranes, western China. International Geology Review, 49, 969–995.

Murthy V. R., Van Westrenen W., and Fei Y.W. (2003) Experimental evidence that potassium is a substantial radioactive heat source in planetary cores. Nature, 423,163–165.

Ogasawara, Y., Fukasawa, K., and Maruyama, S. (2002) Coesite exsolution from titanite in UHP marble from the Kokchetav Massif. American Mineralogist, 87, 452-461.

Oh, C.W., and Liou, J.G. (1998) A petrogenetic grid for eclogite and related facies under high-pressure metamorphism. The Island Arc, 7, 36–51.

Okamoto, K., and Maruyama, S. (1998) Multi-anvil re-equilibration experiments of a Dabie Shan ultrahigh pressure eclogite within the diamond-stability fields. Island Arc, 7, 52–69.

Okamoto, K., and Maruyama, S. (1999) The high-pressure synthesis of lawsonite in the MORB+H2O system. American Mineralogiost, 84 362–373.

Okamoto, K., Liou, J.G., and Ogasawara, Y. (2000) Petrology of the diamond-gradeeclogite in the Kokchetav Massif, northern Kazakhstan. The Island Arc, 9, 379–399.

Peacock, S.M. (1990) Fluid processes in subduction zones. Science, 248, 328-337.

Ravna, E.J.K., and Terry, M.P. (2004) Geothermobarometry of UHP and HP eclogites and schists–an evaluation of equilibria among garnet – clinopyroxene – kyanite – phengite – coesite/quartz. Journal of Metamorphic Geology, 22, 579–592.

Reid, A. M., Brown, R.W., Dawson, J. B., Whitfield, G. G., and Siebert, J. C. (1976) Garnet and pyroxene compositions in some diamondiferous eclogites. Contribution to Mineralogy and Petrology, 58, 203–220.

Schertl, H.P., and Sobolev, N.V. (2013) The Kokchetav Massif, Kazakhstan: ‘‘Type locality’’ of diamond-bearing UHP metamorphic rocks. Journal of Asian Earth Sciences, 63, 5-38.

Schmädicke, E., and Müller,W.F. (2000) Unusual exsolution phenomena in omphacite and partial

replacement of phengite by phlogopite + kyanite in an eclogite from the Erzgebirge. Contributions to Mineralogy and Petrology, 139, 629-642.

Smyth, J.R., Bell, D.R., and Rossman, G.R. (1991) Incorporation of hydroxyl in upper-mantle clinopyroxenes. Nature, 351, 732-735.

Sobolev, N.V., and Shatsky, V.S. (1990) Diamond inclusions in garnets from metamorphic rocks: a new environment for diamond formation. Nature, 343, 742–746.

Song, S. G., Yang, J. S., Liou, J.G., Wu, C. L., Shi, R.D., and Xu, Z.Q. (2003) Petrology, geochemistry and isotopic ages of eclogites from the Dulan UHPM terrane, the North Qaidam, NW China. Lithos, 70, 195–211.

Song, S.G., Zhang, L.F., and Niu, Y.L. (2004) Ultra-deep origin of garnet peridotite from the North Qaidam ultrahigh-pressure belt, Northern Tibetan Plateau, NW China. American Mineralogist, 89, 1330–1336.

Song, S.G., Zhang, L.F., Chen, J., Liou, J.G., and Niu, Y.L. (2005) Sodic amphibole exsolutions in garnet from garnet-peridotite, North Qaidam UHPM belt, NW China: Implications for ultradeep-origin and hydroxyl defects in mantle garnets. American Mineralogist, 90, 814–820.

Schmidt 1996 Experimental Constraints on Recycling of Potassium from Subducted Oceanic Crust. Science, 272, 1927–1930.

Switzer, G., and Melson, W.G. (1969) Partially melted kyanite eclogite from the Roberts Victor mine, South Africa. Smithsonian Contributions to the Earth Sciences, 1, 1-9.

Tsuruta, K., and Takahashi, E. (1998) Melting study of an alkali basalt JB-1 up to 12.5 GPa: behavior of potassium in the deep mantle. Physics of the Earth and Planetary Interiors, 107, 119–130.

Ullemeyer, K., Braunb, G., Dahmsc, M., Kruhld, J.H., Olesene, N.O., and Siegesmunda, S. (2000) Texture analysis of a muscovite-bearing quartzite: a comparison of some currently used techniques. Journal of Structural Geology, 22(11-12), 1541-1557.

Wang, W.Y, and Takahashi, E. (1999) Subsolidus and melting experiments of a K-rich basaltic composition to 27 GPa: Implication for the behavior of potassium in the mantle. American Mineralogist, 84, 357-361.

Whitney, D. L., and Evans, B. W. (2010) Abbreviations for names of rock-forming minerals. American Mineralogist, 95, 185–187.

Xiao, Y., Hoefs, J., van den Kerkhof, A.M., Fiebig, J., and Zheng, Y.F. (2000) Fluids history of UHP metamorphism in Dabie Shan, China: a fluids inclusion and oxygen isotope study on the coesite-bearing eclogite from Bixiling. Contributions to Mineralogy and Petrology, 139, 1–16.

Yang, J.S., Xu, Z.Q., Song, S.G., Zhang, J.X., Wu, C.L., Shi, R.D., Li, H.B., and Maurice, B. (2001) Discovery of coesite in the North Qaidam Early Paleozoic ultrahigh pressure metamorphic belt, NW China. Sciences De La Terre Et Des Planets, 333, 719–724.

Zhang, G.B., Ellis, D.J., Christy, A.G., Zhang, L.F., Niu, Y.L., and Song, S.G. (2009a) UHP metamorphic evolution of coesite-bearing eclogite from the Yuka terrane, North Qaidam UHPM belt, NW China. European Journal of Mineralogy, 21(6), 1287–1300.

Zhang, G.B., Zhang, L.F., Song, S.G., and Niu, Y.L. (2009b) UHP metamorphic evolution and SHRIMP geochronology of a coesite-bearing meta-ophiolitic gabbro in the North Qaidam, NW China. Journal of Asian Earth Sciences, 35(3–4), 310–322.

Zhang, J.X., Meng, F.C., Li, J.P., and Mattinson, C.G. (2009) Coesite in eclogite from the north Qaidam Mountains and its implication. Chinese Science Bulletin, 54, 1105–1110.

Zhang, L.F., Song, S., Liou, J., Ai, Y., and Li, X. (2005) Relict coesite exsolution in omphacite from Western Tianshan eclogites, China. American Mineralogist, 90, 181-186.

Zhou, X.Z. (1997) The discovery of phlogopite exsolution lamellae in garnets of eclogite inclusions, Liaoning Province. Acta Geologica Sinica, 71(1), 33-42.

Zhu, Y.F., and Ogasawara, Y. (2002) Phlogopite and coesite exsolution from super-silicic clinopyroxene. International Geology Review, 44, 831-836.

Figure captions:

FIGURE 1. (a) Schematic map showing major petro-tectonic subunits of the Altun-Qilian-Qaidam orogen, NW China. The red box near Dulan (lower right corner) indicates the location of study area. (b) Geological map of the Yematan UHPM terrane showing the sample locations. Both modified from Song et al. 2003.

FIGURE 2. Photomicrographs showing textures and mineral assemblages of studied eclogites from the Yematan, North Qaidam UHPM belt, NW China. (a) and (b) plane polarized light; (c)-(f) crossed polarized light. (a) (b), Xenoblastic garnet associated with rutile and omphacite in eclogite (a: sample 12ym05; b: sample 11ym26); (c) Phengite exsolution in porphyroblastic omphacite associated with garnet (sample 11ym26); (d) the enlarge of phengite exsolution in omphacite of (c); (e) and (f) Photomicrographs of phengite exsolutions in matrix omphacite (sample 12ym05). Mineral abbreviations are according to Whitney and Evans (2010).

FIGURE 3. P-T diagrams for Ph-exsolved eclogite samples 12ym05 and 11ym26 based on the assemblage Grt + Omp + Ph (for error brackets, see Ravna and Terry 2004).

FIGURE 4. EBSD images of (a) a host omphacite and (b) a phengite lamellae in the host omphacite; (c) and (d) Lattice preferred orientations of phengite and host omphacite.

FIGURE 5. (a) K_2O contents in subsolidus clinopyroxene as a function of pressure along the geothermal gradient in the Earth's mantle. Modified from Wang and Takahashi (1999). (b) The suggested retrograde P–T path of the Yematan UHP eclogites. Thick-black lines are the limits of free water in mid-ocean ridge basalt (MORB) composition (Okamoto and Maruyama 1999). Abbreviations: GS = greenschist facies, EA = epidote-amphibolite facies, Am = amphibolite facies, GR = granulite facies , HGR = high-pressure granulite facies, BS = blueschist facies, AmpEC = amphibole eclogite facies, ZoEC = zoisite eclogite facies, LwsEC = lawsonite eclogite facies, DryEC = dry eclogite facies. Petrogenic grids, subdivision of eclogite facies are from Oh and Liou (1998) and Okamoto and Maruyama (1999), and reaction curves of diamond-graphite,

coesite-quartz, and Phengite-in/out from Blundy (1980), Bohlen and Boettcher (1982) and Auzanneau et al. 2006, respectively.

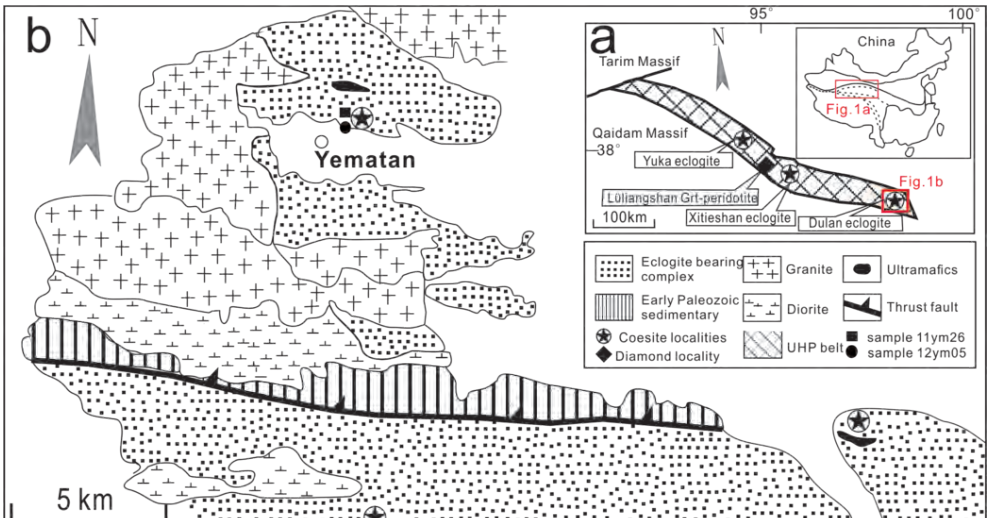
b
N
Yematan
5 km
a
95°
100°
N
Tarim Massif
China
Fig.1a
Qaidam Massif
38°
Yuka eclogite
Fig.1b
Lüliangshan Grt-peridotite
Xitieshan eclogite
Dulan eclogite
100km
Eclogite bearing complex
Granite
Ultramafics
Early Paleozoic sedimentary
Diorite
Thrust fault
Coesite localities
Diamond locality
UHP belt
sample 11ym26
sample 12ym05

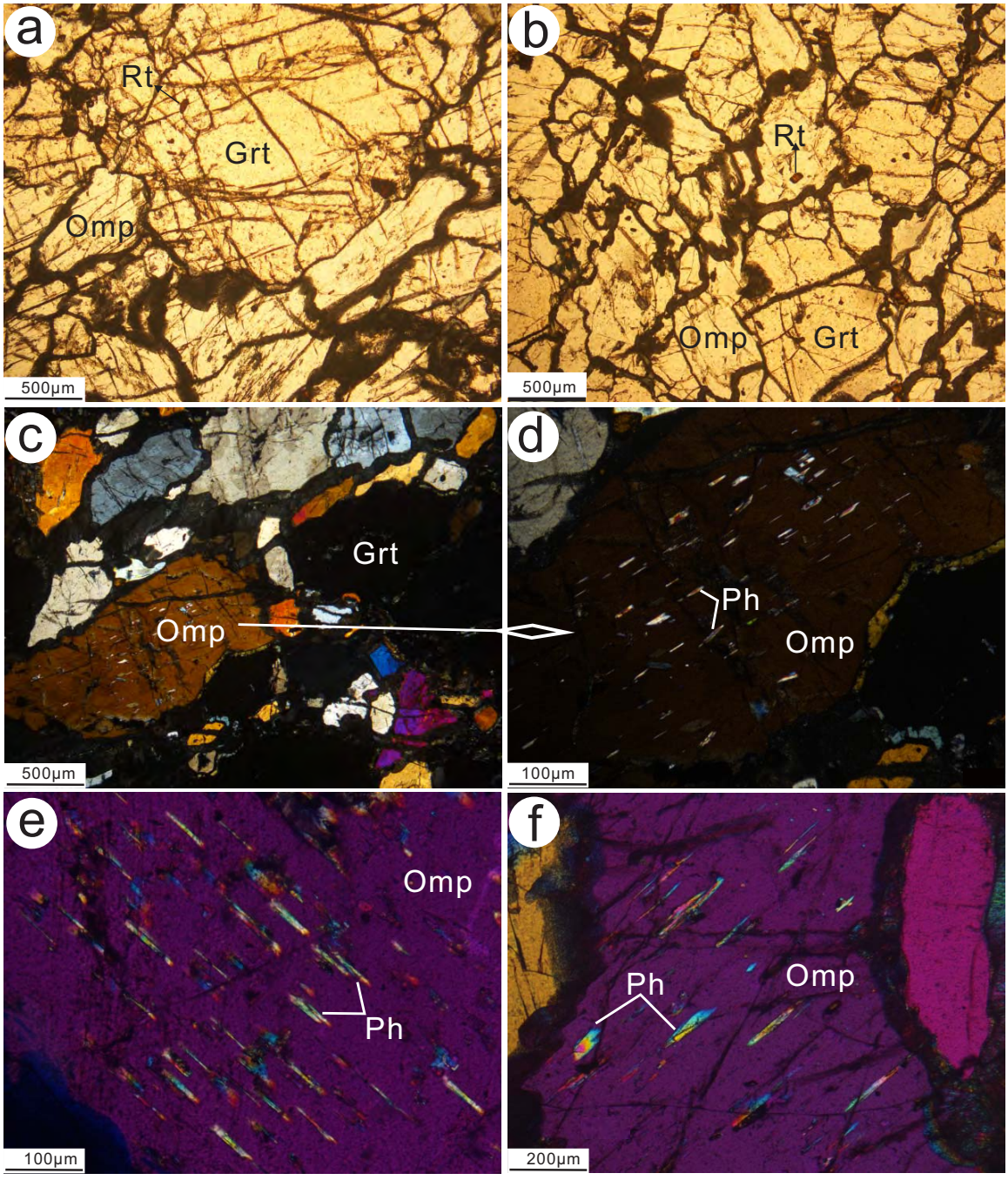
a
Rt
Grt
Omp
500μm
b
Rt
Omp
Grt
500μm
c
Grt
Omp
500μm
d
Ph
Omp
100μm
e
Omp
Ph
100μm
f
Ph
Omp
200μm

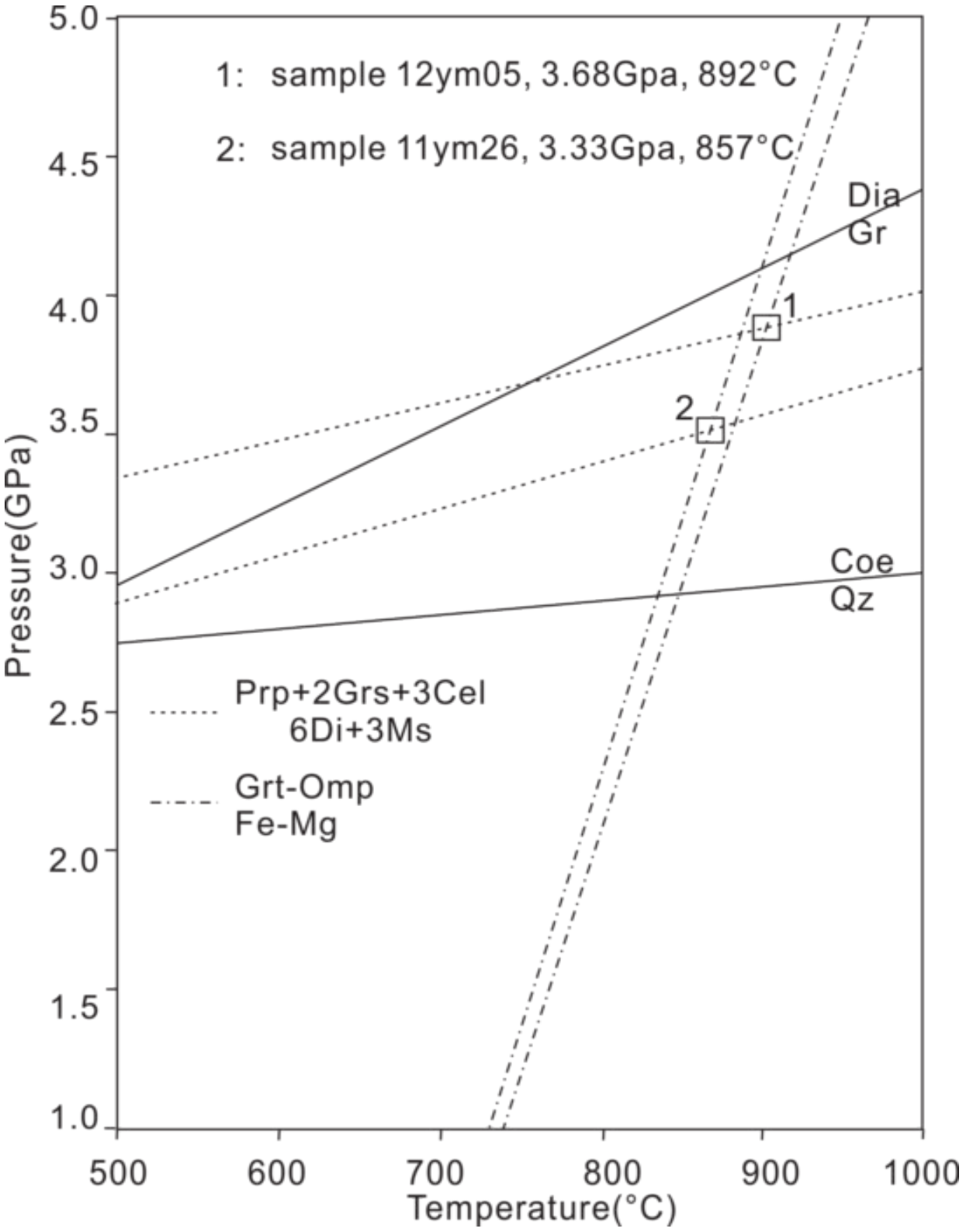
1: sample 12ym05, 3.68Gpa, 892°C
2: sample 11ym26, 3.33Gpa, 857°C
Dia
Gr
Coe
Qz
1
2
Prp+2Grs+3Cel
6Di+3Ms
Grt-Omp
Fe-Mg
Pressure(GPa)
Temperature(°C)
5.0
4.5
4.0
3.5
3.0
2.5
2.0
1.5
1.0
500
600
700
800
900
1000

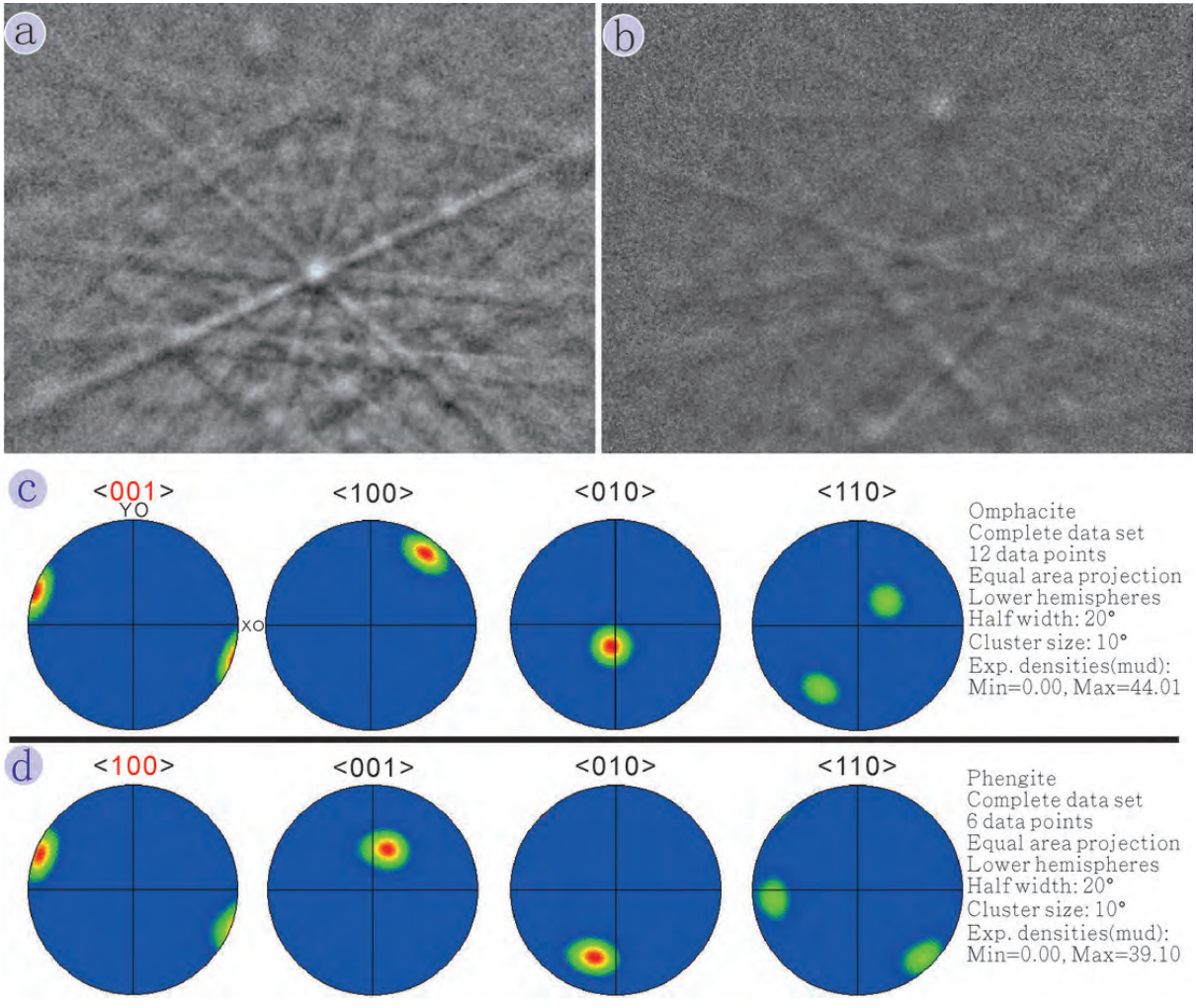
a
b
c
<001>
YO
XO
<100>
<010>
<110>
Omphacite
Complete data set
12 data points
Equal area projection
Lower hemispheres
Half width: 20°
Cluster size: 10°
Exp. densities(mud):
Min=0.00, Max=44.01
d
<100>
<001>
<010>
<110>
Phengite
Complete data set
6 data points
Equal area projection
Lower hemispheres
Half width: 20°
Cluster size: 10°
Exp. densities(mud):
Min=0.00, Max=39.10

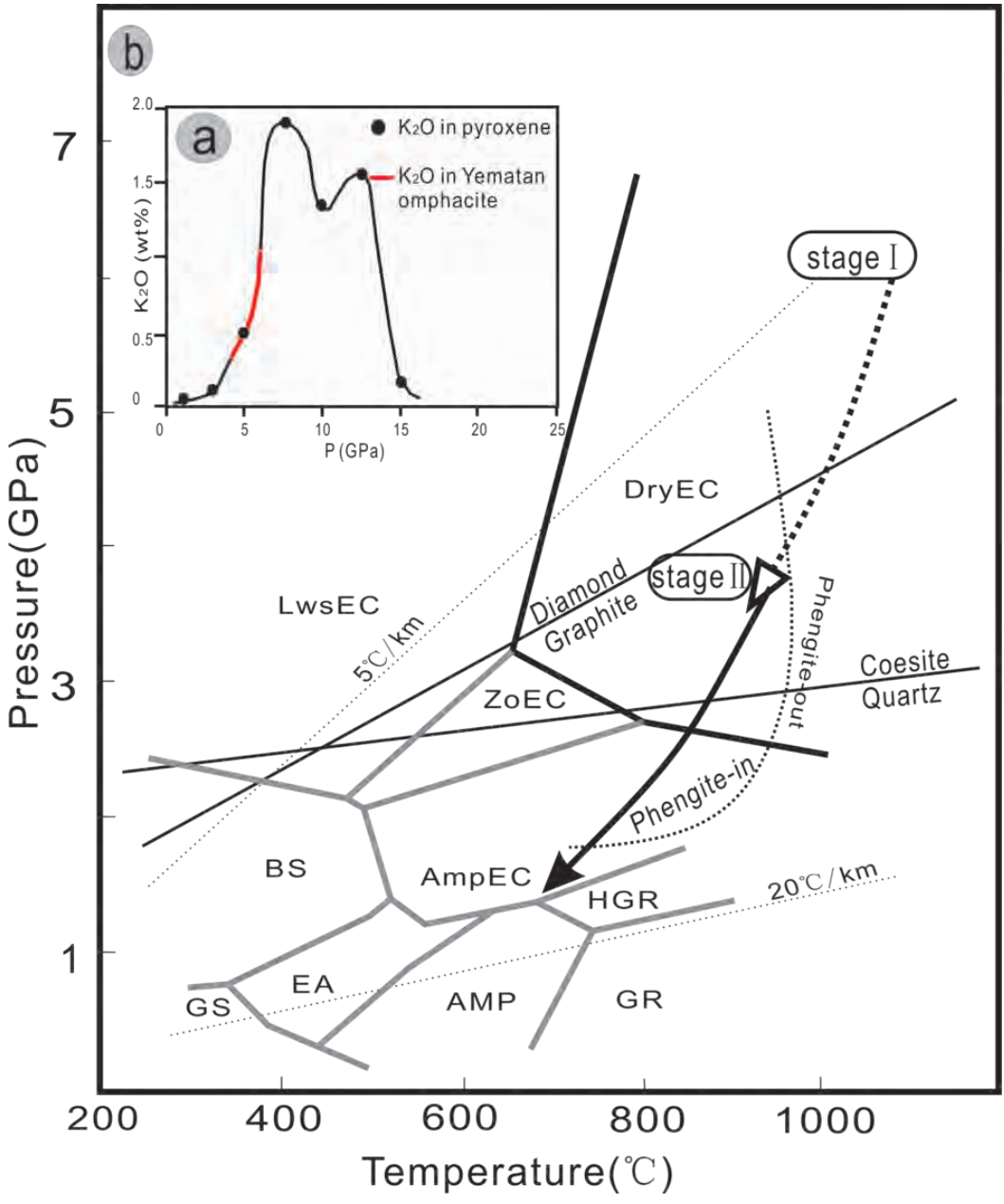
b
a
K2O in pyroxene
K2O in Yematan omphacite
K2O (wt%)
P (GPa)
stage Ⅰ
stage Ⅱ
DryEC
LwsEC
ZoEC
BS
AmpEC
HGR
EA
GS
AMP
GR
Diamond
Graphite
Coesite
Quartz
Phengite-out
Phengite-in
5℃/km
20℃/km
Pressure(GPa)
Temperature(℃)

Table 1. Representative microprobe analyses of garnets.

Sample	12ym05													11ym26								
SiO2	39.37	40.29	39.74	39.90	39.70	39.84	39.88	39.49	39.10	39.97	39.73	39.86	39.33	40.49	38.82	39.90	39.71	39.27	38.87	38.59	38.76	37.87
TiO2	0.00	0.06	0.10	0.10	0.00	0.09	0.08	0.02	0.08	0.09	0.07	0.00	0.00	0.11	0.09	0.00	0.12	0.00	0.16	0.04	0.00	0.05
Al2O3	21.82	23.04	22.94	22.83	22.80	22.84	22.94	22.73	22.91	22.97	22.89	23.05	22.60	23.16	22.12	22.37	22.40	22.57	22.50	22.69	22.40	21.54
Cr2O3	0.04	0.00	0.03	0.00	0.00	0.01	0.03	0.01	0.01	0.03	0.02	0.01	0.01	0.00	0.04	0.01	0.03	0.00	0.02	0.00	0.01	0.00
FeO	16.85	18.89	18.15	19.17	18.95	19.29	18.45	18.55	18.30	18.45	18.51	18.28	18.61	17.54	20.84	20.79	22.22	22.36	20.70	20.21	21.18	21.81
MnO	0.22	0.30	0.46	0.42	0.46	0.62	0.34	0.33	0.29	0.28	0.27	0.25	0.38	0.20	0.48	0.44	0.45	0.48	0.39	0.49	0.37	0.44
MgO	7.73	9.21	8.81	9.08	8.71	8.35	9.21	8.95	9.07	9.22	9.46	9.24	9.01	8.37	6.20	6.46	7.12	6.83	6.22	6.36	6.34	6.18
CaO	11.76	9.72	10.09	9.81	10.16	9.66	9.78	9.83	9.66	9.78	9.81	9.45	9.99	12.00	11.75	10.90	9.44	9.71	11.39	11.31	10.27	10.05
Na2O	0.00	0.01	0.00	0.04	0.02	0.04	0.02	0.05	0.00	0.01	0.05	0.03	0.03	0.04	0.03	0.06	0.01	0.07	0.01	0.00	0.04	0.03
K2O	0.00	0.01	0.00	0.01	0.01	0.00	0.01	0.00	0.02	0.01	0.01	0.00	0.00	0.02	0.01	0.00	0.01	0.00	0.01	0.00	0.02	0.00
Totals	97.79	101.53	100.32	101.36	100.81	100.74	100.74	99.96	99.44	100.81	100.82	100.17	99.96	101.93	100.38	100.93	101.51	101.29	100.27	99.69	99.39	97.97
Si	3.03	2.99	2.99	2.97	2.98	2.99	2.98	2.98	2.96	2.99	2.97	2.99	2.97	2.99	2.97	3.02	3.00	2.97	2.97	2.96	2.99	2.97
Ti	0.00	0.00	0.01	0.01	0.00	0.01	0.00	0.00	0.00	0.01	0.00	0.00	0.00	0.01	0.01	0.00	0.01	0.00	0.01	0.00	0.00	0.00
Al	1.98	2.02	2.03	2.01	2.02	2.02	2.02	2.02	2.05	2.02	2.02	2.04	2.01	2.02	1.99	2.00	1.99	2.02	2.03	2.05	2.04	1.99
Cr	0.00	0.00	0.00	0.00	0.00	0.00	0.00	0.00	0.00	0.00	0.00	0.00	0.00	0.00	0.00	0.00	0.00	0.00	0.00	0.00	0.00	0.00
Fe3	0.00	0.00	0.00	0.04	0.04	0.00	0.01	0.02	0.02	0.00	0.05	0.00	0.06	0.00	0.07	0.00	0.00	0.05	0.01	0.02	0.00	0.06
Fe2	1.09	1.17	1.14	1.15	1.15	1.21	1.15	1.15	1.14	1.15	1.10	1.15	1.11	1.09	1.26	1.32	1.40	1.36	1.31	1.27	1.37	1.37
Mn	0.01	0.02	0.03	0.03	0.03	0.04	0.02	0.02	0.02	0.02	0.02	0.02	0.02	0.01	0.03	0.03	0.03	0.03	0.03	0.03	0.02	0.03
Mg	0.89	1.02	0.99	1.01	0.97	0.94	1.03	1.01	1.02	1.03	1.05	1.03	1.01	0.92	0.71	0.73	0.80	0.77	0.71	0.73	0.73	0.72
Ca	0.97	0.77	0.81	0.78	0.82	0.78	0.78	0.80	0.78	0.78	0.79	0.76	0.81	0.95	0.96	0.88	0.76	0.79	0.93	0.93	0.85	0.85
Na	0.00	0.00	0.00	0.01	0.00	0.01	0.00	0.01	0.00	0.00	0.01	0.01	0.01	0.01	0.01	0.01	0.00	0.01	0.00	0.00	0.01	0.00
K	0.00	0.00	0.00	0.00	0.00	0.00	0.00	0.00	0.00	0.00	0.00	0.00	0.00	0.00	0.00	0.00	0.00	0.00	0.00	0.00	0.00	0.00
Sum	7.98	8.00	7.99	8.00	8.00	7.99	8.00	8.00	8.00	8.00	8.00	7.99	8.00	8.00	8.00	7.99	8.00	8.00	8.00	8.00	8.00	8.00
Alm	0.37	0.39	0.38	0.39	0.39	0.41	0.39	0.39	0.38	0.39	0.37	0.39	0.38	0.37	0.43	0.45	0.47	0.46	0.44	0.43	0.46	0.46
Sps	0.00	0.01	0.01	0.01	0.01	0.01	0.01	0.01	0.01	0.01	0.01	0.01	0.01	0.00	0.01	0.01	0.01	0.01	0.01	0.01	0.01	0.01
Pyp	0.30	0.34	0.33	0.34	0.33	0.32	0.34	0.34	0.35	0.34	0.36	0.35	0.34	0.31	0.24	0.25	0.27	0.26	0.24	0.25	0.25	0.24
Grs	0.33	0.26	0.27	0.26	0.28	0.26	0.26	0.27	0.26	0.26	0.27	0.26	0.27	0.32	0.33	0.30	0.25	0.27	0.31	0.31	0.29	0.29

Note : The cations were calculated using the AX software by Tim Holland, http://www.esc.cam.ac.uk/astaff/holland/ax.html; 12, 11, 6 cations as calculation basis for garnet, phengite, omphacite.

Table 2. Representative EMP analyses of exsolution lamellae-hosting omphacites.

Sample	12ym05									11ym26								
SiO2	56.00	55.30	55.51	55.23	55.13	55.35	52.58	55.38	54.15	55.52	55.16	55.31	55.28	55.90	55.72	56.26	55.62	55.53
TiO2	0.22	0.11	0.21	0.05	0.10	0.17	0.10	0.07	0.01	0.14	0.14	0.07	0.00	0.12	0.09	0.03	0.18	0.08
Al2O3	9.11	10.02	10.71	10.62	10.56	10.62	10.36	10.44	10.97	12.35	13.13	12.24	12.75	12.75	13.17	12.43	12.89	12.50
Cr2O3	0.06	0.03	0.00	0.02	0.00	0.04	0.03	0.08	0.03	0.01	0.01	0.02	0.03	0.03	0.03	0.00	0.00	0.00
FeO	3.76	3.48	3.48	3.49	3.46	3.50	3.71	3.34	4.22	4.76	4.77	4.79	4.69	4.18	4.44	4.59	4.60	5.02
MnO	0.03	0.04	0.05	0.02	0.00	0.04	0.05	0.00	0.06	0.00	0.08	0.03	0.01	0.00	0.00	0.02	0.00	0.03
MgO	10.31	10.28	10.52	10.52	10.26	10.24	10.59	10.30	9.07	8.15	7.46	8.17	8.08	7.79	7.71	7.93	7.80	7.96
CaO	16.02	15.40	15.66	16.04	15.91	15.57	15.98	15.80	14.22	12.66	12.06	12.81	12.51	12.48	12.57	12.44	12.47	12.43
Na2O	4.96	5.74	5.90	6.02	6.12	6.30	5.92	5.87	6.50	7.92	8.11	7.30	7.90	7.46	7.79	7.86	7.87	7.84
K2O	0.08	0.05	0.00	0.00	0.00	0.00	0.00	0.02	0.01	0.00	0.01	0.00	0.02	0.00	0.00	0.00	0.00	0.00
Totals	100.50	100.20	101.70	102.00	101.50	101.80	99.30	101.00	99.30	101.50	100.90	100.40	101.30	100.50	101.20	101.20	101.00	101.40
Si	1.99	1.96	1.93	1.93	1.93	1.93	1.90	1.94	1.94	1.94	1.94	1.95	1.93	1.96	1.94	1.96	1.94	1.94
Ti	0.01	0.00	0.01	0.00	0.00	0.01	0.00	0.00	0.00	0.00	0.00	0.00	0.00	0.00	0.00	0.00	0.01	0.00
Al	0.38	0.42	0.44	0.44	0.44	0.44	0.44	0.43	0.46	0.51	0.54	0.51	0.53	0.53	0.54	0.51	0.53	0.52
Cr	0.00	0.00	0.00	0.00	0.00	0.00	0.00	0.00	0.00	0.00	0.00	0.00	0.00	0.00	0.00	0.00	0.00	0.00
Fe3	0.00	0.06	0.08	0.09	0.09	0.09	0.10	0.08	0.11	0.12	0.12	0.09	0.12	0.05	0.10	0.10	0.11	0.13
Fe2	0.11	0.04	0.01	0.01	0.01	0.01	0.01	0.01	0.01	0.01	0.01	0.04	0.01	0.07	0.02	0.02	0.01	0.01
Mn	0.00	0.00	0.00	0.00	0.00	0.00	0.00	0.00	0.00	0.00	0.00	0.00	0.00	0.00	0.00	0.00	0.00	0.00
Mg	0.55	0.54	0.55	0.55	0.54	0.53	0.57	0.54	0.48	0.42	0.39	0.43	0.42	0.41	0.40	0.41	0.41	0.41
Ca	0.61	0.58	0.58	0.60	0.60	0.58	0.62	0.59	0.55	0.47	0.45	0.48	0.47	0.47	0.47	0.46	0.47	0.47
Na	0.34	0.39	0.40	0.41	0.42	0.43	0.41	0.40	0.45	0.54	0.55	0.50	0.54	0.51	0.53	0.53	0.53	0.53
K	0.00	0.00	0.00	0.00	0.00	0.00	0.00	0.00	0.00	0.00	0.00	0.00	0.00	0.00	0.00	0.00	0.00	0.00
Sum	3.99	4.00	4.00	4.01	4.01	4.01	4.04	4.00	4.00	4.01	4.01	4.00	4.01	4.00	4.00	4.00	4.00	4.00
Jd	38.74	38.34	37.98	36.15	36.29	36.63	32.49	37.66	40.32	44.31	47.56	46.48	45.77	50.31	48.44	47.24	47.09	45.78

Table 3. Representative EMP analyses of phengite lamellae.

Sample	12ym05							11ym26						
SiO2	52.60	59.56	53.99	54.62	56.75	55.44	55.67	55.80	55.70	55.94	55.47	55.31	55.08	54.95
TiO2	0.62	0.51	0.71	0.66	0.42	0.39	0.51	0.85	0.60	0.64	0.63	1.08	1.13	0.99
Al2O3	27.55	25.71	28.27	28.88	28.06	27.75	28.15	28.33	28.20	28.82	28.95	29.03	28.58	28.96
Cr2O3	0.00	0.06	0.01	0.04	0.07	0.06	0.06	0.01	0.00	0.02	0.00	0.00	0.00	0.00
FeO	1.27	1.14	1.19	1.26	1.34	1.08	1.07	1.62	1.26	1.22	1.83	1.44	1.73	1.68
MnO	0.01	0.05	0.00	0.00	0.02	0.04	0.00	0.04	0.03	0.02	0.01	0.02	0.04	0.00
MgO	3.60	2.76	3.75	3.77	4.15	4.08	4.11	3.79	4.02	3.81	3.81	3.56	3.78	3.63
CaO	0.08	2.35	0.05	0.20	0.03	0.06	0.10	0.16	0.08	0.09	0.13	0.14	0.24	0.14
Na2O	0.74	2.17	0.60	0.60	0.71	0.55	0.75	0.52	0.40	0.68	0.61	0.41	0.61	0.45
K2O	6.79	5.60	7.61	8.10	7.27	7.12	7.15	5.72	6.90	7.05	5.16	6.42	5.85	6.16
Totals	93.26	99.91	96.18	98.13	98.82	96.57	97.57	96.84	97.19	98.29	96.60	97.41	97.04	96.96
Si	3.47	3.67	3.47	3.45	3.53	3.53	3.51	3.51	3.51	3.50	3.49	3.48	3.47	3.47
Ti	0.03	0.02	0.03	0.03	0.02	0.02	0.02	0.04	0.03	0.03	0.03	0.05	0.05	0.05
Al	2.14	1.87	2.14	2.15	2.06	2.08	2.09	2.10	2.10	2.12	2.15	2.15	2.12	2.16
Cr	0.00	0.00	0.00	0.00	0.00	0.00	0.00	0.00	0.00	0.00	0.00	0.00	0.00	0.00
Fe3	0.05	0.00	0.04	0.04	0.05	0.04	0.04	0.06	0.04	0.04	0.06	0.05	0.06	0.06
Fe2	0.02	0.06	0.02	0.03	0.02	0.02	0.02	0.02	0.02	0.02	0.03	0.02	0.03	0.03
Mn	0.00	0.00	0.00	0.00	0.00	0.00	0.00	0.00	0.00	0.00	0.00	0.00	0.00	0.00
Mg	0.35	0.25	0.36	0.36	0.39	0.39	0.39	0.36	0.38	0.36	0.36	0.33	0.36	0.34
Ca	0.01	0.16	0.00	0.01	0.00	0.00	0.01	0.01	0.01	0.01	0.01	0.01	0.02	0.01
Na	0.10	0.26	0.07	0.07	0.09	0.07	0.09	0.06	0.05	0.08	0.08	0.05	0.08	0.06
K	0.57	0.44	0.62	0.65	0.58	0.58	0.58	0.46	0.56	0.56	0.41	0.51	0.47	0.50
Sum	6.74	6.73	6.76	6.79	6.73	6.72	6.74	6.63	6.69	6.72	6.62	6.66	6.66	6.65